An update on ozone profile trends for the period 2000 to 2016

Wolfgang Steinbrecht[1], Lucien Froidevaux[2], Ryan Fuller[2], Ray Wang[3], John Anderson[4], Chris Roth[5], Adam Bourassa[5], Doug Degenstein[5], Robert Damadeo[6], Joe Zawodny[6], Stacey Frith[7,8], Richard McPeters[7], Pawan Bhartia[7], Jeannette Wild[9,10], Craig Long[9], Sean Davis[11,12], Karen Rosenlof[11], Viktoria Sofieva[13], Kaley Walker[14], Nabiz Rahpoe[15], Alexei Rozanov[15], Mark Weber[15], Alexandra Laeng[16], Thomas von Clarmann[16], Gabriele Stiller[16], Natalya Kramarova[7,8], Sophie Godin-Beekmann[17], Thierry Leblanc[18], Richard Querel[19], Daan Swart[20], Ian Boyd[21], Klemens Hocke[22], Niklaus Kämpfer[22], Eliane Maillard Barras[23], Lorena Moreira[22], Gerald Nedoluha[24], Corinne Vigouroux[25], Thomas Blumenstock[16], Matthias Schneider[16], Omaira García[26], Nicholas Jones[27], Emmanuel Mahieu[28], Dan Smale[19], Michael Kotkamp[19], John Robinson[19], Irina Petropavlovskikh[29,12], Neil Harris[30], Birgit Hassler[31], Daan Hubert[25], and Fiona Tummon[32]

[1]Deutscher Wetterdienst, Hohenpeissenberg, Germany
[2]Jet Propulsion Laboratory, California Institute of Technology, Pasadena, CA, USA
[3]School of Earth and Atmospheric Sciences, Georgia Institute of Technology, Atlanta, GA, USA
[4]Department of Atmospheric and Planetary Sciences, Hampton University, Hampton, VA, USA
[5]Institute of Space and Atmospheric Studies, University of Saskatchewan, Saskatoon, Canada
[6]NASA Langley Research Center, Hampton, VA, USA
[7]NASA Goddard Space Flight Center, Silver Spring, MD, USA
[8]Science Systems and Applications Inc., Lanham, MD, USA
[9]NOAA/NWS/NCEP/Climate Prediction Center, College Park, MD, USA
[10]Innovim LLC, Greenbelt, MD, USA
[11]Chemical Sciences Division, NOAA ESRL, Boulder, CO, USA
[12]CIRES, University of Colorado, Boulder, CO, USA
[13]Finnish Meteorological Institute, Helsinki, Finland
[14]Department of Physics, University of Toronto, Canada
[15]Institute for Environmental Physics, University of Bremen, Germany
[16]Karlsruhe Institute of Technology, Institute of Meteorology and Climate Research, Karlsruhe, Germany
[17]Centre National de la Recherche Scientifique, Université de Versailles Saint-Quentin-en-Yvelines, Guyancourt, France
[18]Jet Propulsion Laboratory, California Institute of Technology, Wrightwood, CA, USA
[19]National Institute of Water and Atmospheric Research (NIWA), Lauder, New Zealand
[20]National Institute for Public Health and the Environment (RIVM), Bilthoven, The Netherlands
[21]BC Scientific Consulting LLC, Stony Brook, NY, USA
[22]Institute of Applied Physics and Oeschger Centre for Climate Change Research, University of Bern, Switzerland
[23]MeteoSwiss, Payerne, Switzerland
[24]Naval Research Laboratory, Washington, D.C., USA
[25]Royal Belgian Institute for Space Aeronomy (BIRA-IASB), Brussels, Belgium
[26]Izaña Atmospheric Research Centre (IARC), Agencia Estatal de Meteorología (AEMET), Santa Cruz de Tenerife, Spain
[27]School of Chemistry, University of Wollongong, Australia
[28]Institute of Astrophysics and Geophysics, University of Liège, Belgium
[29]Climate Monitoring Division, NOAA ESRL, Boulder, CO, USA
[30]Centre for Atmospheric Informatics and Emissions Technology, Cranfield University, United Kingdom
[31]Bodeker Scientific, Alexandra, New Zealand
[32]ETH Zürich, Switzerland

Correspondence to: Wolfgang Steinbrecht (wolfgang.steinbrecht@dwd.de)

Abstract. Ozone profile trends over the period 2000 to 2016 from several merged satellite ozone data sets and from ground-based data by four techniques at stations of the Network for the Detection of Atmospheric Composition Change indicate significant ozone increases in the upper stratosphere, between 35 and 48 km altitude (5 and 1 hPa). Near 2 hPa (42 km), ozone has been increasing by about 1.5% per decade in the tropics (20°S to 20°N), and by 2 to 2.5% per decade in the 35° to 60°

5 latitude bands of both hemispheres. At levels below 35 km (5 hPa), 2000 to 2016 ozone trends are smaller and not statistically significant. The observed trend profiles are consistent with expectations from chemistry climate model simulations. Using three to four more years of observations and updated data sets, this study confirms positive trends of upper stratospheric ozone already reported, e.g., in the WMO/UNEP Ozone Assessment 2014, or by Harris et al. (2015). The additional years, and the fact that nearly all individual data sets indicate these increases, give enhanced confidence. Nevertheless, a thorough analysis

10 of possible drifts and differences between various data sources is still required, as is a detailed attribution of the observed increases to declining ozone depleting substances and to stratospheric cooling. Ongoing quality observations from multiple independent platforms are key for verifying that recovery of the ozone layer continues as expected.

1 Introduction

Depletion of the stratospheric ozone layer by anthropogenic chlorine and bromine from ozone depleting substances (ODS)

15 has been a world-wide concern since the 1970s (Stolarski and Cicerone, 1974; Molina and Rowland, 1974). Initially, studies predicted the largest ozone losses for the upper stratosphere, at about 42 km or 2 hPa (Crutzen, 1974). For the total column of ozone only moderate losses were predicted. The situation changed dramatically with the discovery of the Antarctic ozone hole (Chubachi, 1984; Farman et al., 1985). The ozone hole is characterized by large ozone depletion throughout the lower stratosphere, which is due to heterogeneous reactions on the surface of Polar Stratospheric Clouds (Solomon, 1999). These

20 important reactions had not been known or not been included in the early predictions. Thus, the large spring-time ozone losses over an entire continent were a huge surprise. The world's nations reacted by signing the International Vienna Convention for the Protection of the Ozone layer (1985), and by implementing the 1987 Montreal Protocol and its later amendments. Thanks to these agreements, the world-wide production and consumption of ODS have been eliminated almost completely since the early 1990s (WMO, 2007).

25 The Montreal Protocol has been very successful. The concentration of ODS in the atmosphere has been declining since the mid-1990s in the troposphere, and since the late 1990s also in the stratosphere (WMO, 2011). Scientific assessments of the state of the ozone layer have shown that the ozone layer is responding: The decline of ozone in the upper stratosphere stopped around 2000 (Newchurch et al., 2003; WMO, 2007). Total ozone columns have also stabilized (WMO, 2011, 2014). Given the current slow decline of ODS concentrations, we now expect ozone to increase accordingly in the stratosphere.

30 The last WMO/UNEP ozone assessment (WMO, 2014) concluded that statistically significant increases of ozone had been observed only in the upper stratosphere (around 42 km or 2 hPa), but not at lower levels, and not for total ozone columns.

About half of the increase in the upper stratosphere was attributed to declining ODS, the other half to declining temperature. This stratospheric cooling is caused by increasing CO_2 (Jonsson et al., 2004; Randel et al., 2016). Low temperature enhances ozone in the upper stratosphere, by slowing gas-phase destruction cycles and making ozone production more efficient.

Studies published after WMO (2014) have confirmed this tendency of ozone increasing in the upper stratosphere, but they also pointed out that uncertainties might be larger and upward trends might not be statistically different from zero (Harris et al., 2015; Hubert et al., 2016). The purpose of the present paper is to follow up on WMO (2014), using the same methodology, but with three to four more years of data, and with improved and additional data sets. Here we present initial results. For the future, a more comprehensive investigation of instrumental and merging uncertainties, and of uncertainties for different regression analyses is planned in the "Long-term Ozone Trends and Uncertainties in the Stratosphere" initiative (LOTUS), which has been started by the Stratosphere-troposphere Processes And their Role in Climate project (SPARC) of the World Climate Research Programme (WCRP), see http://www.sparc-climate.org/activities/ozone-trends/.

2   Ozone Profile Data Records

Only a few long-term records of ozone profile data start before 1990 and extend past 2014 to the present (see also Tegtmeier et al., 2013; Hassler et al., 2014; Tummon et al., 2015). Tables 1 and 2 summarize the merged satellite records and ground-based stations used in the present study.

The nadir viewing Solar Backscatter UltraViolet (SBUV) instruments on NASA and NOAA satellites have measured ozone profiles continuously since late 1978, covering the sunlit part of the globe, but with only coarse altitude resolution of 10 to 15 kilometers (McPeters et al., 2013). Orbit drifts, differences between individual instruments, instrument degradation, and some other problems require careful assessment, when generating a long-term data set from these measurements. Currently two SBUV based data sets (Version 8.60) are available: The merged SBUV MOD (release 6) ozone data set generated by NASA (Frith et al., 2014), termed SBUV-NASA in the following, and the "coherent" SBUV data set generated by NOAA (Wild and Long, 2017), termed SBUV-NOAA in the following.

Ozone profiles with higher vertical resolution (about 2 km), but also with sparser coverage, were provided by the satellite-borne Stratospheric Aerosol and Gas Experiments (SAGE) and the Halogen Occultation Experiment (HALOE). These instruments measured in solar occultation geometry from 1979 to about 1982, from late 1984 to 2005, and from 1991 to 2005, respectively (Damadeo et al., 2013, 2014; Remsberg, 2008). Since 2002, the Optical Spectrograph and InfraRed Imaging System (OSIRIS) measures ozone profiles from ultraviolet light scattered in limb geometry (McLinden et al., 2012). SAGE II and OSIRIS ozone profiles have been combined by Bourassa et al. (2014) to produce a long-term data set, which has subsequently been improved. Optionally, this data set also includes ozone profiles from the limb viewing instrument of the Ozone Mapping Profiler Suite (OMPS), which has operated since early 2012 (e.g., Flynn et al., 2014).

Using microwave emissions in limb geometry, the Microwave Limb Sounder (MLS) on the Aura satellite has been measuring many stratospheric trace gases since 2004, including ozone profiles with dense spatial sampling and a vertical resolution of 2.5 to 3 km in the stratosphere (Waters et al., 2006). SAGE, HALOE, ACE-FTS (= Atmospheric Chemistry Experiment Fourier

Transform Spectrometer, see Bernath, 2017) and MLS ozone profiles have been combined in the Global OZone Chemistry And Related trace gas Data records for the Stratosphere (GOZCARDS, Froidevaux et al., 2015) and in the Stratospheric Water and OzOne Satellite Homogenized data set (SWOOSH, Davis et al., 2016).

For the period from August 2002 to April 2012, ozone profiles were measured by the SCIAMACHY (= SCanning Imaging

5   Absorption spectroMeter for Atmospheric CHartographY), GOMOS (= Global Ozone Monitoring by Occultation of Stars) and MIPAS (= Michelson Interferometer for Passive Atmospheric Sounding) instruments on board the European ENVISAT satellite. Positive ozone trends have been reported in the upper stratosphere for each of these instruments (Gebhardt et al., 2014; Kyrölä et al., 2013; Eckert et al., 2014). Unfortunately, ENVISAT failed in April 2012, and measurements ceased. The ESA Climate Change Initiative has generated a harmonized ozone profile data set from the ENVISAT instruments, the SMR (=

10 Sub-Millimeter Radiometer) microwave instrument, the OSIRIS instrument, and ACE-FTS (Sofieva et al., 2013; Rahpoe et al., 2015). This "ESA CCI" or "Ozone CCI" ozone profile record has recently been updated and extended, with SAGE II ozone profiles back to 1984, and with OMPS ozone profiles (2D retrieval from U. Saskatoon) from 2012 to the present (SAGE + CCI + OMPS, see Sofieva et al., 2017). Another new merged data set, following previous work by Laeng et al. (2016), combines the MIPAS (Fischer et al., 2008) ozone profile record (KIT/IMK processing) with the records from SAGE II and OMPS (NASA v2

15 retrieval). Because of short or lacking overlap periods, this SAGE + MIPAS + OMPS record relies on ACE-FTS as a transfer standard for matching MIPAS high spectral resolution mode data (07/2002 until 03/2004) to MIPAS low spectral resolution mode data (01/2005 to 04/2012), and for matching the latter to OMPS data (after 02/2012).

The longest ground-based ozone profile records for the upper stratosphere come from Dobson spectrometers operated in "Umkehr" mode (Petropavlovskikh et al., 2005, 2011). Umkehr ozone profiles have coarse altitude resolution, about 10 km.

20 Long-term ground-based measurements of ozone in the upper stratosphere are also available from the Network for the Detection of Atmospheric Composition Change (NDACC, http://www.ndacc.org, Kurylo et al., 2016). These measurements started in the late 1980s and 1990s, using differential absorption lidars, microwave radiometers (Steinbrecht et al., 2009), and Fourier transform infrared spectrometers (FTIRs, Vigouroux et al., 2015). FTIR ozone profiles have coarse altitude resolution (8 to 15 km) and resolve only 3 layers in the stratosphere. Altitude resolution for the microwave radiometers is also 8 to 15 km. Lidars

25 provide altitude resolution between 1 km (below 30 km) and 10 km (above 45 km). Note, however, that altitude resolution is not that important for the investigation of long-term trends in the upper stratosphere, which are usually coherent over a wide range of altitudes and latitudes (different, however, for changes around the tropopause). Table 2 summarizes the ground-based stations used in the present study.

A comprehensive intercomparison of limb-viewing satellite instruments with ground-based NDACC instruments by Hubert

30 et al. (2016) indicates that SAGE II and Aura-MLS, the primary instruments in many of the merged records, are very stable. If drifts exist, they are smaller than $\pm 2\%$ per decade in the 20 to 40 km region, and not statistically significant. Below 20 km and above 45 km uncertainties become larger, because of larger geophysical variation in the compared altitude ranges, and because of increasing measurement errors, see also Tegtmeier et al. (2013). Note that in Hubert et al. (2016), the OSIRIS V5.07 ozone data did exhibit a significant drift, up to 8% per decade near 40 km. This drift has been corrected in the revised and updated

35 OSIRIS V5.10 data set used here. Drifts of most SBUV instruments are less than 3 to 5% per decade, and are not statistically

significant (Kramarova et al., 2013). Similarly, Rahpoe et al. (2015) report that drifts of several limb viewing instruments including ACE-FTS, MIPAS, and OSIRIS are typically less than 3% per decade (even for older processing versions), and not statistically significant.

Figure 1 shows annual mean ozone anomalies from the different satellite and ground-based data sets, averaged over three latitude bands, and for a level near 2 hPa or 42 km. Anomalies are relative to the 1998 to 2008 climatology of each individual data set. All data sets show clear ozone declines until the late 1990s, and show generally increasing ozone over the 2000 to 2016 period, especially at mid-latitudes. This observed evolution generally confirms expectations from model simulations by Chemistry Climate Models within their Validation-2 initiative (CCMVal-2, Eyring et al., 2010, grey lines in Fig. 1). The simulations attribute the ozone decline until the late 1990s to increasing ODS loading, and predict positive ozone trends due to declining ODS loading since around 2000. In the simulations, the ozone increase is enhanced by overall cooling of the stratosphere due to increasing greenhouse gases (see also Jonsson et al., 2004; Randel et al., 2016).

All observational data sets show similar fluctuations from year to year, usually within 1 or 2% of each other. They also indicate similar long-term tendencies, usually within ±2% per decade of each other, and comparable to the CCMVal-2 simulations. Generally, the station data show larger variations than the zonal means from the satellite data. This is not surprising, given the sparser sampling of most ground-based data (lidar, Umkehr, and FTIR all require clear sky). Geophysical differences between a station location and the wide-band zonal means are also possible.

3 Multiple Linear Regression

Multiple linear regression (MLR) has become a standard method for deriving ozone trends (Bojkov et al., 1990; Reinsel et al., 2002; Newchurch et al., 2003; Chehade et al., 2014). MLR can be applied to monthly mean ozone anomaly time series $dO_3(i)$ of many months i. The anomalies are obtained by referencing the monthly mean $O_3(i)$ to the climatological mean for each calendar month $O_{3,Clim}(i \bmod 12)$.

$$dO_3(i) = \frac{O_3(i) - O_{3,Clim}(i \bmod 12)}{O_{3,Clim}(i \bmod 12)} \tag{1}$$

MLR attempts to reconstruct the observed anomalies as a linear combination of prescribed predictors $P_j(i)$, which account for known ozone variations, and residual noise $\epsilon(i)$.

$$dO_3(i) = c_0 + \sum_{j=1}^{n} c_j * P_j(i) + \epsilon(i) \tag{2}$$

Here our set of predictors P_j includes a linear trend, a change of the trend in January 1997 (hockey stick), two proxies for the Quasi-Biennial Oscillation (QBO) and a proxy for the 11-year solar cycle Reinsel et al. (as in 2002). Like WMO (2014) or Harris et al. (2015), the present study also includes a proxy for stratospheric aerosol loading and for El-Nino / La Nina, which is most relevant for the tropical lower stratosphere (e.g., Oman et al., 2013). Table 3 summarizes the proxies used, and their

sources. Other studies may include further proxies for weather patterns and meridional ozone transports, such as circulation indices or eddy heat flux (Steinbrecht et al., 2001; Reinsel et al., 2005), but this was not done here. The coefficients c_j are obtained by least squares fitting of the residuals, i.e. minimization of $\sum_i \epsilon^2(i)$. Typically, the residuals $\epsilon(i)$ are of the order of 1 to 10%, large enough to cover fit errors and measurement errors for each monthly mean.

5   If realistic uncertainties $\Delta O_3(i)$ are available for each monthly mean, the anomalies can be weighted by their inverse squared uncertainty (high weight for low uncertainty), and the uncertainties $\Delta O_3(i)$ can be used to estimate the uncertainty Δc_j of the fitted c_j. However, in many cases reliable uncertainties are not available for monthly means, because it is difficult to account correctly for all error terms, and for autocorrelation and covariance of the individual measurement errors (e.g., Toohey and von Clarmann, 2013; Damadeo et al., 2014). A time-invariant bias, for example, might be included in the monthly mean uncertainty,
10 but it would be irrelevant for the long-term trend. So in many studies, including Reinsel et al. (2005), WMO (2014), Harris et al. (2015), and this study, the pragmatic approach is to use the standard deviation of the fit residuals $\epsilon(i)$ for estimating the uncertainties Δc_j of the fitted coefficients.

Strictly, the uncertainties from the MLR assume that the predictors are orthogonal, and that the residuals $\epsilon(i)$ are uncorrelated white noise. In practice, the predictors above are orthogonal enough (cross-correlations less than 0.3 for the long periods considered), and first order auto-correlation in the residuals is small ($|AC| \ll 0.3$). Still, to correct for first order auto-correlation
15 AC (Reinsel et al., 2002), the Δc_j are multiplied here by $\sqrt{(1+AC)/(1-AC)}$. Neglecting higher orders of autocorrelation might result in slightly underestimated uncertainties (Vyushin et al., 2007).

One problem with the "hockey stick" fit is that the slope of the declining trend and the time of the turning point have an influence on the slope of the second part of the "hockey stick" (Reinsel et al., 2002). To reduce this problem, a second step
20 was introduced in WMO (2014), and is also used here. First, Equation 2 is used to estimate QBO, solar cycle, aerosol and El Nino effects over the entire record. These latter effects are then subtracted from the ozone anomalies, resulting in ozone residuals $O_{3,res}(i)$ which include the long-term trend component, other remaining variability and the $\epsilon(i)$. Then, in a second step, a simple linear trend is fitted to the $O_{3,res}(i)$. This trend can be fitted over any desired period, here 2000 to 2016, since QBO, solar cycle and ENSO related variations have already been taken care of. The second fit is not constrained as much by
25 the "hockey stick" assumption, and has more freedom to react to the remaining ozone variations over the desired period.

4   Ozone Profile Trends

4.1   Trends for individual data sets

Figures 2 and 3 present the latitude-pressure cross-sections of 2000 to 2016 ozone trends TR (and uncertainties σ) obtained using the two-step method from the previous section for the satellite-based data sets from Section 2. In addition, the top right
30 panel shows corresponding trends for the CCMVal-2 simulations. The magnitude of the trends is represented by the color scale. Grey shading indicates regions where trends are not statistically significant (95% confidence level, $|TR| \leq 2\sigma$). All satellite data sets show significant ozone increases in the upper stratosphere, above 10 to 5 hPa (30 to 35 km). At levels between 50 and 10 hPa (20 and 30 km), trends are generally not significant, except for islands of significant trends near 20 hPa or 50 hPa

in some data sets, mostly in the southern hemisphere. Most data sets (but not SAGE + MIPAS + OMPS) also show significant ozone decline in the tropical lowermost stratosphere below 100 hPa (16 km). However, satellite measurements in this region can have large uncertainties and need very careful consideration, both in tropics and extra-tropics.

The simulations (in the top right panel of Fig. 2) confirm that significant trends should be expected only in the upper stratosphere, between 10 and 0.5 hPa (30 to 55 km). Exactly there, the observed data sets give significant increasing trends. Both magnitude - between 1 and 5% per decade - and latitudinal pattern - smaller increases in the tropics, larger increases at higher latitudes - are consistent between the satellite data sets and the simulations.

Figs. 2 and 3, therefore, provide substantial observational evidence for significant ozone increases in the upper stratosphere, consistent with model simulations based on declining ODS and decreasing temperatures in the upper stratosphere. Comparison of Figs. 2 and 3 with Figure 2-10 of WMO (2014) shows that the addition of three more years of data, as well as improved and additional data sets, have not changed the overall picture very much.

A specific look at zonal mean trends from all satellite and ground-based data sets is given in Fig. 4. The basis for these trend calculations are the zonal band anomaly time series as in Fig. 1. In Fig. 4, almost all individual data sets show increasing ozone between 5 and 1 hPa, with trends between 0 and 4% per decade. For the 5 and 2 hPa levels, the plotted $\pm 2\sigma$ uncertainty bars (from the MLR) indicate that most individual trends are statistically significant (95% confidence level). Between 50 and 10 hPa (22 and 30 km), most data sets indicate small and non-significant trends. In the lowermost stratosphere, between 100 and 50 hPa (16 and 22 km), several data sets report ozone decreases, but these are generally not statistically significant. Differences between data sets are larger as well. Overall, Fig. 4 confirms significant ozone increases in the upper stratosphere, whereas ozone trends at lower levels are generally smaller and not significant.

4.2 From individual data set trends to the average trend

To compare with other studies, or with model simulations, it is useful to obtain an average ozone trend profile from all individual trends. In WMO (2014) this was done by a weighted mean of all individual ground-based and satellite trends $TR(i)$. Each individual trend was weighted with its inverse squared uncertainty $(1/\sigma(i))^2$, so more uncertain trends have less weight. Individual uncertainties $\sigma(i)$ came from the regression (as in Section 3), and also included a 1 or 2% per decade drift uncertainty (2σ, depending on the instrument) added in quadrature. This standard weighted mean approach (SWM) was also used in Harris et al. (2015), however, with much larger drift uncertainties (6% per decade, 2σ), resulting in larger overall uncertainty and in non-significant trends compared to WMO (2014). One problem with the standard weighted mean is that its uncertainty does not depend on the spread of the individual trends (because of Gaussian error propagation). Therefore, Harris et al. (2015) also considered the joint distribution approach (J). There, the uncertainty of the mean trend is essentially given by the standard deviation of the individual trends σ, divided by $\sqrt{n}$, where n is the number of data sets. Strictly, n should be the number of statistically independent realizations. Since most merged data sets use the same SBUV, SAGE, MLS, or OMPS instruments, these data sets are not independent. Also, the multiple linear regression uses the same approach and the same proxies for all data sets, which may further reduce independence between the individual trend estimates.

Given these caveats, Fig. 5 shows the joint distribution trends (black lines), obtained here by averaging the seven satellite data sets (GOZCARDS, SWOOSH, SAGE + OSIRIS, SAGE + CCI + OMPS, SAGE + MIPAS + OMPS, SBUV-NASA, and SBUV-NOAA). All were given the same weight, and SBUV data were used only at levels above 40 hPa (23 km). The (joint distribution) uncertainty bars give ± 2 standard deviations over all seven data sets. Using these uncertainty bars in the Figure

5 assumes only 1 independent realization ($n = 1$), and should give a very conservative uncertainty estimate for the mean trend TR. Even with this conservative uncertainty estimate, significant increasing trends ($|TR| \geq 2\sigma$) appear in Fig. 5 for the 2 hPa level in the tropics and at northern mid-latitudes. Table 4 gives the same trend results, but now bold letters indicate trends TR, that are significant with 95% confidence ($|TR| \geq 2\sigma/\sqrt{n}$), assuming $n = 3$ independent realizations, or $n = 2$ below 40 hPa. In this less conservative case, significant increasing trends appear nearly everywhere above 10 hPa (30 km). As mentioned

10 above, trends at 70 hPa (and below) differ more between data sets and should be considered with care. See also the large error bars below 50 hPa for the tropical latitudes in Fig. 5.

For comparison, the yellow lines and shading in Fig. 5 show average 1998 to 2012 trends and uncertainties from Harris et al. (2015), and the blue lines give average 2000 to 2013 trends and error bars from WMO (2014). Overall, the updated 2000 to 2016 trend profiles (black lines) agree quite well with Harris et al. (2015) and with WMO (2014), especially when the

15 overlapping error bars are considered. The major difference is the substantially larger uncertainty range reported in Harris et al. (2015) for the upper stratosphere. This probably caused by two outlying data sets: 1.) An older version of the SAGE + OSIRIS data set, where the OSIRIS (V5.07) data suffered from a large drift (Hubert et al., 2016). 2.) A now outdated SAGE + GOMOS data set, which exhibited unrealistically low / negative trends at latitudes poleward of 45° (see Fig. 5 of Harris et al., 2015). For levels above 5 hPa (35 km) and levels below 30 hPa (25 km), the new and improved merged satellite data sets, and the

20 additional years, provide substantially smaller trend uncertainties than Harris et al. (2015). In particular, there is no indication that the new merged satellite data sets differ by more than 1 or 2% per decade due to instrumental drifts, at levels above 50 hPa. Compared to WMO (2014), the current work reports slightly larger uncertainty bars. This is expected, because the standard weighted mean uncertainty used in WMO (2014) did not consider the spread of the individual trends (as mentioned above), and assumed statistical independence for all data sets in their average.

25 The updated trend profiles in Fig. 5 also show excellent agreement with the CCMVal-2 simulations, with virtually no difference at levels above 50 hPa (20 km). The fact that all individual data sets in Fig. 4 indicate significant increases in the upper stratosphere, the reduced uncertainty since Harris et al. (2015), the excellent agreement with the CCMVal-2 simulations in Fig. 5, and the good agreement with trend results from WMO (2014), all give enhanced confidence that ozone is indeed increasing in the upper stratosphere, and that at least part of the increase is due to declining ODS.

30 5 Conclusions

New and improved satellite data sets, and the addition of data after 2013 until the end of 2016, improve our confidence that ozone in the upper stratosphere, between 5 and 1 hPa (35 to 48 km), has been increasing since 2000. Between 50 and 10 hPa (20 to 30 km) trends are small, and there are no clear indications for increasing (or decreasing) ozone. In the lowermost

stratosphere, between 100 and 50 hPa (16 and 20 km), there might be an indication for decreasing ozone in the tropics and at northern mid-latitudes. However, differences between data sets in this region are larger. Instrumental difficulties and large natural variability require more careful analysis of these possible ozone decreases.

Overall, the updated ozone profile trends are consistent with previous studies, e.g. with WMO (2014) and Harris et al. (2015).

5 Using the average 2000 to 2016 trend from seven continuing and improved satellite data sets, and their standard deviation as uncertainty, trend uncertainty in the upper stratosphere is reduced by a factor of two compared to Harris et al. (2015). Ozone increases at the 2 hPa (42 km) level are statistically significant with more than 90 or 95% confidence over a wide range of latitudes. In addition, the majority of all individual satellite and ground-based data sets also indicates significant ozone increases at levels above 10 hPa.

10 There are, however, remaining questions, for example regarding the merging of different instrumental records, the quality of the records in the lowermost stratosphere, or on the best methods for trend estimation and their detailed uncertainties. These issues are being addressed in the "Long-term Ozone Trends and Uncertainties in the Stratosphere" (LOTUS) initiative, which runs under the Stratosphere-troposphere Processes And their Role in Climate project (SPARC) of the World Climate Research Programme (WCRP), see http://www.sparc-climate.org/activities/ozone-trends/. The goals of LOTUS are to further improve

15 the data sets, to better understand all relevant uncertainties, and to achieve a more complete and more precise picture of trends in the stratospheric ozone profile.

The update presented here, however, already gives strong indications that ozone in the upper stratosphere has been increasing over the last 15 years, and has begun to recover from man-made ozone depleting substances. Simulations show that this process will take many more decades. In order to verify that ozone recovery continues as expected, reliable long-term observations from

20 multiple independent platforms will remain crucial for many years to come.

Author contributions. The paper was written by W. Steinbrecht, who also did the trend analysis, and is responsible for the NDACC lidar measurements at Hohenpeissenberg. L. Froidevaux, R. Fuller, H.J. Wang, and J. Anderson contributed the GOZCARDS data set, R.P. Damadeo, J.M. Zawodny, A. Bourassa, C. Roth, and D. Degenstein the SAGE + OSIRIS + OMPS data set, S. Frith, R.S. Stolarski, R.D. McPeters, and P.K. Bhartia the SBUV-NASA data set and OMPS data, J. Wild and C. Long the SBUV-NOAA data set, S. Davis and K. Rosenlof the

25 SWOOSH data set, V. Sofieva, K. Walker, N. Rahpoe A. Rozanov, M. Weber and others the SAGE + ESA CCI + OMPS data set, and A. Laeng, T. von Clarmann, G. Stiller and N. Kramarova the SAGE + MIPAS + OMPS data set. NDACC lidar measurements were provided by S. Godin-Beekmann, T. Leblanc, R. Querel, and D.P.J. Swart. NDACC microwave measurements were given by I. Boyd, K. Hocke, N. Kämpfer, E. Maillard, L. Moreira, and G. Nedoluha. C. Vigouroux, T. Blumenstock, M. Schneider, O. García, N. Jones, E. Mahieu, D. Smale, M. Kotkamp, and J. Robinson provided the NDACC FTIR data. I. Petropavlovskikh and E. Maillard Barras processed the Umkehr data set.

30 N.R.P. Harris, B. Hassler, D. Hubert, and F. Tummon contributed important input and discussions on trends, data sets, and their uncertainties.

Acknowledgements. The authors gratefully acknowledge the extremely important contribution from staff at the stations, who run and fix the ground-based systems, and from the many people involved in the satellite measurements. Funding by national and supra-national agencies is also gratefully acknowledged. OHP NDACC lidar measurements are funded by CNRS and CNES. Work performed at the Jet Propulsion

Laboratory, California Institute of Technology, was done under contract with the National Aeronautics and Space Administration. NOAA supports and funds a major part of the Dobson Umkehr measurements, in collaboration with funding and work done by Meteoswiss, Switzerland; NIWA, New Zealand; the Australian Bureau of Meteorology; CNRS, France; and the University of Fairbanks, Alaska. We acknowledge the CCMVal-2 group for providing their model simulations. Fiona Tummon was supported by Swiss National Science Foundation grant number 20FI21_138017.

References

Bernath, P. F.: The Atmospheric Chemistry Experiment (ACE), J. Quant. Spectr. Rad. Tran., 186, 3–16, doi:10.1016/j.jqsrt.2016.04.006, http://doi.org/10.1016/j.jqsrt.2016.04.006, 2017.

Bojkov, R., Bishop, L., Hill, W. J., Reinsel, G. C., and Tiao, G. C.: A statistical trend analysis of revised Dobson total ozone data over the Northern Hemisphere, J. Geophys. Res., 95, 9785–9807, doi:10.1029/JD095iD07p09785, http://dx.doi.org/10.1029/JD095iD07p09785, 1990.

Bourassa, A. E., Degenstein, D. A., Randel, W. J., Zawodny, J. M., Kyrölä, E., McLinden, C. A., Sioris, C. E., and Roth, C. Z.: Trends in stratospheric ozone derived from merged SAGE II and Odin-OSIRIS satellite observations, Atmos. Chem. Phys., 14, 6983–6994, doi:10.5194/acp-14-6983-2014, http://www.atmos-chem-phys.net/14/6983/2014/, 2014.

Chehade, W., Weber, M., and Burrows, J. P.: Total ozone trends and variability during 1979–2012 from merged data sets of various satellites, Atmos. Chem. Phys., 14, 7059–7074, doi:10.5194/acp-14-7059-2014, http://www.atmos-chem-phys.net/14/7059/2014/, 2014.

Chubachi, S.: A Special Ozone Observation at Syowa Station, Antarctica, from February 1982 to January 1983, Atmospheric Ozone, D. Reidel, Norwell, Mass., 00, 285–289, 1984.

Crutzen, P. J.: Estimates of possible future ozone reductions from continued use of fluoro-chloro-methanes (CF2Cl2, CFCl3), Geophys. Res. Lett., 1, 205–208, doi:10.1029/GL001i005p00205, http://dx.doi.org/10.1029/GL001i005p00205, 1974.

Damadeo, R. P., Zawodny, J. M., Thomason, L. W., and Iyer, N.: SAGE version 7.0 algorithm: application to SAGE II, Atmos. Meas. Tech., 6, 3539–3561, doi:10.5194/amt-6-3539-2013, http://www.atmos-meas-tech.net/6/3539/2013/, 2013.

Damadeo, R. P., Zawodny, J. M., and Thomason, L. W.: Reevaluation of stratospheric ozone trends from SAGE II data using a simultaneous temporal and spatial analysis, Atmos. Chem. Phys., 14, 13455–13470, doi:10.5194/acp-14-13455-2014, http://www.atmos-chem-phys. net/14/13455/2014/, 2014.

Davis, S. M., Rosenlof, K. H., Hassler, B., Hurst, D. F., Read, W. G., Vömel, H., Selkirk, H., Fujiwara, M., and Damadeo, R.: The Stratospheric Water and Ozone Satellite Homogenized (SWOOSH) database: A long-term database for climate studies, Earth Syst. Sci. Data, 8, 461–490, doi:10.5194/essd-8-461-2016, http://www.earth-syst-sci-data.net/8/461/2016/, 2016.

Eckert, E., von Clarmann, T., Kiefer, M., Stiller, G. P., Lossow, S., Glatthor, N., Degenstein, D. A., Froidevaux, L., Godin-Beekmann, S., Leblanc, T., McDermid, S., Pastel, M., Steinbrecht, W., Swart, D. P. J., Walker, K. A., and Bernath, P. F.: Drift-corrected trends and periodic variations in MIPAS IMK/IAA ozone measurements, Atmos. Chem. Phys., 14, 2571–2589, doi:10.5194/acp-14-2571-2014, http://www.atmos-chem-phys.net/14/2571/2014/, 2014.

Eyring, V., Cionni, I., Bodeker, G. E., Charlton-Perez, A. J., Kinnison, D. E., Scinocca, J. F., Waugh, D. W., Akiyoshi, H., Bekki, S., Chipperfield, M. P., Dameris, M., Dhomse, S., Frith, S. M., Garny, H., Gettelman, A., Kubin, A., Langematz, U., Mancini, E., Marchand, M., Nakamura, T., Oman, L. D., Pawson, S., Pitari, G., Plummer, D. A., Rozanov, E., Shepherd, T. G., Shibata, K., Tian, W., Braesicke, P., Hardiman, S. C., Lamarque, J. F., Morgenstern, O., Pyle, J. A., Smale, D., and Yamashita, Y.: Multi-model assessment of stratospheric ozone return dates and ozone recovery in CCMVal-2 models, Atmos. Chem. Phys., 10, 9451–9472, doi:10.5194/acp-10-9451-2010, http://www.atmos-chem-phys.net/10/9451/2010/, 2010.

Farman, J. C., Gardiner, B. G., and Shanklin, J. D.: Large losses of total ozone in Antarctica reveal seasonal ClOx/NOx interaction, Nature, 315, 207–210, doi:10.1038/315207a0, http://dx.doi.org/10.1038/315207a0, 1985.

Fischer, H., Birk, M., Blom, C., Carli, B., Carlotti, M., von Clarmann, T., Delbouille, L., Dudhia, A., Ehhalt, D., Endemann, M., Flaud, J. M., Gessner, R., Kleinert, A., Koopman, R., Langen, J., López-Puertas, M., Mosner, P., Nett, H., Oelhaf, H., Perron, G., Remedios, J.,

Ridolfi, M., Stiller, G., and Zander, R.: MIPAS: An instrument for atmospheric and climate research, Atmos. Chem. Phys., 8, 2151–2188, doi:10.5194/acp-8-2151-2008, http://www.atmos-chem-phys.net/8/2151/2008/, 2008.

Flynn, L., Long, C., Wu, X., Evans, R., Beck, C. T., Petropavlovskikh, I., McConville, G., Yu, W., Zhang, Z., Niu, J., Beach, E., Hao, Y., Pan, C., Sen, B., Novicki, M., Zhou, S., and Seftor, C.: Performance of the Ozone Mapping and Profiler Suite (OMPS) products, J. Geophys. Res., 119, 6181–6195, doi:10.1002/2013JD020467, http://dx.doi.org/10.1002/2013JD020467, 2013JD020467, 2014.

Frith, S. M., Kramarova, N. A., Stolarski, R. S., McPeters, R. D., Bhartia, P. K., and Labow, G. J.: Recent changes in total column ozone based on the SBUV Version 8.6 Merged Ozone Data Set, J. Geophys. Res., 119, 9735–9751, doi:10.1002/2014JD021889, http://dx.doi.org/10.1002/2014JD021889, 2014JD021889, 2014.

Froidevaux, L., Anderson, J., Wang, H.-J., Fuller, R. A., Schwartz, M. J., Santee, M. L., Livesey, N. J., Pumphrey, H. C., Bernath, P. F., Russell III, J. M., and McCormick, M. P.: Global OZone Chemistry And Related trace gas Data records for the Stratosphere (GOZCARDS): Methodology and sample results with a focus on HCl, H_2O, and O_3, Atmos. Chem. Phys., 15, 10 471–10 507, doi:10.5194/acp-15-10471-2015, http://www.atmos-chem-phys.net/15/10471/2015/, 2015.

Gebhardt, C., Rozanov, A., Hommel, R., Weber, M., Bovensmann, H., Burrows, J. P., Degenstein, D., Froidevaux, L., and Thompson, A. M.: Stratospheric ozone trends and variability as seen by SCIAMACHY from 2002 to 2012, Atmos. Chem. Phys., 14, 831–846, doi:10.5194/acp-14-831-2014, http://www.atmos-chem-phys.net/14/831/2014/, 2014.

Harris, N. R. P., Hassler, B., Tummon, F., Bodeker, G. E., Hubert, D., Petropavlovskikh, I., Steinbrecht, W., Anderson, J., Bhartia, P. K., Boone, C. D., Bourassa, A., Davis, S. M., Degenstein, D., Delcloo, A., Frith, S. M., Froidevaux, L., Godin-Beekmann, S., Jones, N., Kurylo, M. J., Kyrölä, E., Laine, M., Leblanc, S. T., Lambert, J.-C., Liley, B., Mahieu, E., Maycock, A., de Mazière, M., Parrish, A., Querel, R., Rosenlof, K. H., Roth, C., Sioris, C., Staehelin, J., Stolarski, R. S., Stübi, R., Tamminen, J., Vigouroux, C., Walker, K. A., Wang, H. J., Wild, J., and Zawodny, J. M.: Past changes in the vertical distribution of ozone – part 3: Analysis and interpretation of trends, Atmos. Chem. Phys., 15, 9965–9982, doi:10.5194/acp-15-9965-2015, http://www.atmos-chem-phys.net/15/9965/2015/, 2015.

Hassler, B., Petropavlovskikh, I., Staehelin, J., August, T., Bhartia, P. K., Clerbaux, C., Degenstein, D., Mazière, M. D., Dinelli, B. M., Dudhia, A., Dufour, G., Frith, S. M., Froidevaux, L., Godin-Beekmann, S., Granville, J., Harris, N. R. P., Hoppel, K., Hubert, D., Kasai, Y., Kurylo, M. J., Kyrölä, E., Lambert, J.-C., Levelt, P. F., McElroy, C. T., McPeters, R. D., Munro, R., Nakajima, H., Parrish, A., Raspollini, P., Remsberg, E. E., Rosenlof, K. H., Rozanov, A., Sano, T., Sasano, Y., Shiotani, M., Smit, H. G. J., Stiller, G., Tamminen, J., Tarasick, D. W., Urban, J., van der A, R. J., Veefkind, J. P., Vigouroux, C., von Clarmann, T., von Savigny, C., Walker, K. A., Weber, M., Wild, J., and Zawodny, J. M.: Past changes in the vertical distribution of ozone - part 1: Measurement techniques, uncertainties and availability, Atmos. Meas. Tech., 7, 1395–1427, doi:10.5194/amt-7-1395-2014, http://www.atmos-meas-tech.net/7/1395/2014/, 2014.

Hubert, D., Lambert, J.-C., Verhoelst, T., Granville, J., Keppens, A., Baray, J.-L., Bourassa, A. E., Cortesi, U., Degenstein, D. A., Froidevaux, L., Godin-Beekmann, S., Hoppel, K. W., Johnson, B. J., Kyrölä, E., Leblanc, T., Lichtenberg, G., Marchand, M., McElroy, C. T., Murtagh, D., Nakane, H., Portafaix, T., Querel, R., Russell III, J. M., Salvador, J., Smit, H. G. J., Stebel, K., Steinbrecht, W., Strawbridge, K. B., Stübi, R., Swart, D. P. J., Taha, G., Tarasick, D. W., Thompson, A. M., Urban, J., van Gijsel, J. A. E., Van Malderen, R., von der Gathen, P., Walker, K. A., Wolfram, E., and Zawodny, J. M.: Ground-based assessment of the bias and long-term stability of 14 limb and occultation ozone profile data records, Atmos. Meas. Tech., 9, 2497–2534, doi:10.5194/amt-9-2497-2016, http://www.atmos-meas-tech.net/9/2497/2016/, 2016.

Jonsson, A. I., de Grandpré, J., Fomichev, V. I., McConnell, J. C., and Beagley, S. R.: Doubled CO2-induced cooling in the middle atmosphere: Photochemical analysis of the ozone radiative feedback, J. Geophys. Res., 109, n/a–n/a, doi:10.1029/2004JD005093, http://dx.doi.org/10.1029/2004JD005093, d24103, 2004.

Kramarova, N. A., Frith, S. M., Bhartia, P. K., McPeters, R. D., Taylor, S. L., Fisher, B. L., Labow, G. J., and DeLand, M. T.: Validation of ozone monthly zonal mean profiles obtained from the version 8.6 Solar Backscatter Ultraviolet algorithm, Atmos. Chem. Phys., 13, 6887–6905, doi:10.5194/acp-13-6887-2013, http://www.atmos-chem-phys.net/13/6887/2013/, 2013.

Kurylo, M. J., Thompson, A. M., and De Mazière, M.: The Network for the Detection of Atmospheric Composition Change: 25 Years Old and Going Strong, The Earth Observer, 28, 4–15, https://eospso.gsfc.nasa.gov/earthobserver/sep-oct-2016, 2016.

Kyrölä, E., Laine, M., Sofieva, V., Tamminen, J., Päivärinta, S.-M., Tukiainen, S., Zawodny, J., and Thomason, L.: Combined SAGE II–GOMOS ozone profile data set for 1984-2011 and trend analysis of the vertical distribution of ozone, Atmos. Chem. Phys., 13, 10 645–10 658, doi:10.5194/acp-13-10645-2013, http://www.atmos-chem-phys.net/13/10645/2013/, 2013.

Laeng, A., von Clarmann, T., Stiller, G., Dinelli, B. M., Dudhia, A., Raspollini, P., Glatthor, N., Grabowski, U., Sofieva, V., Froidevaux, L., Walker, K., and Zehner, C.: Merged ozone profiles from four MIPAS Processors, Atmos. Meas. Tech. Disc., 2016, 1–14, doi:10.5194/amt-2016-239, http://www.atmos-meas-tech-discuss.net/amt-2016-239/, 2016.

McLinden, C. A., Bourassa, A. E., Brohede, S., Cooper, M., Degenstein, D. A., Evans, W. J. F., Gattinger, R. L., Haley, C. S., Llewellyn, E. J., Lloyd, N. D., Loewen, P., Martin, R. V., McConnell, J. C., McDade, I. C., Murtagh, D., Rieger, L., von Savigny, C., Sheese, P. E., Sioris, C. E., Solheim, B., and Strong, K.: OSIRIS: A Decade of Scattered Light, Bull. Amer. Meteorol. Soc., 93, 1845–1863, doi:10.1175/BAMS-D-11-00135.1, http://dx.doi.org/10.1175/BAMS-D-11-00135.1, 2012.

McPeters, R. D., Bhartia, P. K., Haffner, D., Labow, G. J., and Flynn, L.: The version 8.6 SBUV ozone data record: An overview, J. Geophys. Res., 118, 8032–8039, doi:10.1002/jgrd.50597, http://dx.doi.org/10.1002/jgrd.50597, 2013.

Molina, M. J. and Rowland, F. S.: Stratospheric sink for chlorofluoromethanes: Chlorine atom-catalysed destruction of ozone, Nature, 249, 810–812, doi:10.1038/249810a0, http://dx.doi.org/10.1038/249810a0, 1974.

Newchurch, M. J., Yang, E.-S., Cunnold, D. M., Reinsel, G. C., Zawodny, J. M., and Russell, J. M.: Evidence for slowdown in stratospheric ozone loss: First stage of ozone recovery, J. Geophys. Res., 108, n/a–n/a, doi:10.1029/2003JD003471, http://dx.doi.org/10.1029/2003JD003471, 4507, 2003.

Oman, L. D., Douglass, A. R., Ziemke, J. R., Rodriguez, J. M., Waugh, D. W., and Nielsen, J. E.: The ozone response to ENSO in Aura satellite measurements and a chemistry-climate simulation, J. Geophys. Res., 118, 965–976, doi:10.1029/2012JD018546, http://dx.doi.org/10.1029/2012JD018546, 2013.

Petropavlovskikh, I., Bhartia, P. K., and DeLuisi, J.: New Umkehr ozone profile retrieval algorithm optimized for climatological studies, Geophys. Res. Lett., 32, n/a–n/a, doi:10.1029/2005GL023323, http://dx.doi.org/10.1029/2005GL023323, l16808, 2005.

Petropavlovskikh, I., Evans, R., McConville, G., Oltmans, S., Quincy, D., Lantz, K., Disterhoft, P., Stanek, M., and Flynn, L.: Sensitivity of Dobson and Brewer Umkehr ozone profile retrievals to ozone cross-sections and stray light effects, Atmos. Meas. Tech., 4, 1841–1853, doi:10.5194/amt-4-1841-2011, http://www.atmos-meas-tech.net/4/1841/2011/, 2011.

Rahpoe, N., Weber, M., Rozanov, A. V., Weigel, K., Bovensmann, H., Burrows, J. P., Laeng, A., Stiller, G., von Clarmann, T., Kyrölä, E., Sofieva, V. F., Tamminen, J., Walker, K., Degenstein, D., Bourassa, A. E., Hargreaves, R., Bernath, P., Urban, J., and Murtagh, D. P.: Relative drifts and biases between six ozone limb satellite measurements from the last decade, Atmos. Meas. Tech., 8, 4369–4381, doi:10.5194/amt-8-4369-2015, http://www.atmos-meas-tech.net/8/4369/2015/, 2015.

Randel, W. J., Smith, A. K., Wu, F., Zou, C.-Z., and Qian, H.: Stratospheric Temperature Trends over 1979–2015 derived from combined SSU, MLS, and SABER Satellite Observations, J. Clim., 29, 4843–4859, doi:10.1175/JCLI-D-15-0629.1, http://dx.doi.org/10.1175/JCLI-D-15-0629.1, 2016.

Reinsel, G. C., Weatherhead, E., Tiao, G. C., Miller, A. J., Nagatani, R. M., Wuebbles, D. J., and Flynn, L. E.: On detection of turnaround and recovery in trend for ozone, J. Geophys. Res., 107, ACH 1–1–ACH 1–12, doi:10.1029/2001JD000500, http://dx.doi.org/10.1029/2001JD000500, 2002.

Reinsel, G. C., Miller, A. J., Weatherhead, E. C., Flynn, L. E., Nagatani, R. M., Tiao, G. C., and Wuebbles, D. J.: Trend analysis of total ozone data for turnaround and dynamical contributions, J. Geophys. Res., 110, n/a–n/a, doi:10.1029/2004JD004662, http://dx.doi.org/10.1029/2004JD004662, d16306, 2005.

Remsberg, E. E.: On the response of Halogen Occultation Experiment (HALOE) stratospheric ozone and temperature to the 11-year solar cycle forcing, J. Geophys. Res., 113, n/a–n/a, doi:10.1029/2008JD010189, http://dx.doi.org/10.1029/2008JD010189, d22304, 2008.

Sato, M., Hansen, J. E., McCormick, M. P., and Pollack, J. B.: Stratospheric aerosol optical depths, 1850–1990, J. Geophys. Res., 98, 22 987–22 994, doi:10.1029/93JD02553, http://dx.doi.org/10.1029/93JD02553, 1993.

Sofieva, V. F., Rahpoe, N., Tamminen, J., Kyrölä, E., Kalakoski, N., Weber, M., Rozanov, A., von Savigny, C., Laeng, A., von Clarmann, T., Stiller, G., Lossow, S., Degenstein, D., Bourassa, A., Adams, C., Roth, C., Lloyd, N., Bernath, P., Hargreaves, R. J., Urban, J., Murtagh, D., Hauchecorne, A., Dalaudier, F., van Roozendael, M., Kalb, N., and Zehner, C.: Harmonized dataset of ozone profiles from satellite limb and occultation measurements, Earth Syst. Sci. Data, 5, 349–363, doi:10.5194/essd-5-349-2013, http://www.earth-syst-sci-data.net/5/349/2013/, 2013.

Sofieva, V. F., Rahpoe, N., Tamminen, J., Kyrölä, E., Kalakoski, N., Weber, M., Rozanov, A., von Savigny, C., Laeng, A., von Clarmann, T., Stiller, G., Lossow, S., Degenstein, D., Bourassa, A., Adams, C., Roth, C., Lloyd, N., Bernath, P., Hargreaves, R. J., Murtagh, D., Hauchecorne, A., Dalaudier, F., van Roozendael, M., Kalb, N., and Zehner, C.: Merged SAGE II, Ozone_cci and OMPS ozone profiles dataset and evaluation of ozone trends in the stratosphere, Atmos. Meas. Tech. Disc., QOS 2016 special issue, in preparation, 2017.

Solomon, S.: Stratospheric ozone depletion: A review of concepts and history, Rev. Geophys., 37, 275–316, doi:10.1029/1999RG900008, http://dx.doi.org/10.1029/1999RG900008, 1999.

Steinbrecht, W., Claude, H., Köhler, U., and Winkler, P.: Interannual changes of total ozone and Northern Hemisphere circulation patterns, Geophys. Res. Lett., 28, 1191–1194, doi:10.1029/1999GL011173, http://dx.doi.org/10.1029/1999GL011173, 2001.

Steinbrecht, W., Claude, H., Schönenborn, F., McDermid, I. S., Leblanc, T., Godin-Beekmann, S., Keckhut, P., Hauchecorne, A., Gijsel, J. A. E. V., Swart, D. P. J., Bodeker, G. E., Parrish, A., Boyd, I. S., Kämpfer, N., Hocke, K., Stolarski, R. S., Frith, S. M., Thomason, L. W., Remsberg, E. E., Savigny, C. V., Rozanov, A., and Burrows, J. P.: Ozone and temperature trends in the upper stratosphere at five stations of the Network for the Detection of Atmospheric Composition Change, Int. J. Remote Sens., 30, 3875–3886, doi:10.1080/01431160902821841, http://dx.doi.org/10.1080/01431160902821841, 2009.

Stolarski, R. S. and Cicerone, R. J.: Stratospheric Chlorine: A Possible Sink for Ozone, Can. J. Chem., 52, 1610–1615, doi:10.1139/v74-233, http://dx.doi.org/10.1139/v74-233, 1974.

Tegtmeier, S., Hegglin, M. I., Anderson, J., Bourassa, A., Brohede, S., Degenstein, D., Froidevaux, L., Fuller, R., Funke, B., Gille, J., Jones, A., Kasai, Y., Krüger, K., Kyrölä, E., Lingenfelser, G., Lumpe, J., Nardi, B., Neu, J., Pendlebury, D., Remsberg, E., Rozanov, A., Smith, L., Toohey, M., Urban, J., von Clarmann, T., Walker, K. A., and Wang, R. H. J.: SPARC Data Initiative: A comparison of ozone climatologies from international satellite limb sounders, J. Geophys. Res., 118, 12,229–12,247, doi:10.1002/2013JD019877, http://dx.doi.org/10.1002/2013JD019877, 2013JD019877, 2013.

Toohey, M. and von Clarmann, T.: Climatologies from satellite measurements: the impact of orbital sampling on the standard error of the mean, Atmos. Meas. Tech., 6, 937–948, doi:10.5194/amt-6-937-2013, http://www.atmos-meas-tech.net/6/937/2013/, 2013.

Tummon, F., Hassler, B., Harris, N. R. P., Staehelin, J., Steinbrecht, W., Anderson, J., Bodeker, G. E., Bourassa, A., Davis, S. M., Degenstein, D., Frith, S. M., Froidevaux, L., Kyrölä, E., Laine, M., Long, C., Penckwitt, A. A., Sioris, C. E., Rosenlof, K. H., Roth, C., Wang, H.-J., and Wild, J.: Intercomparison of vertically resolved merged satellite ozone data sets: Interannual variability and long-term trends, Atmos. Chem. Phys., 15, 3021–3043, doi:10.5194/acp-15-3021-2015, http://www.atmos-chem-phys.net/15/3021/2015/, 2015.

5 Vigouroux, C., Blumenstock, T., Coffey, M., Errera, Q., García, O., Jones, N. B., Hannigan, J. W., Hase, F., Liley, B., Mahieu, E., Mellqvist, J., Notholt, J., Palm, M., Persson, G., Schneider, M., Servais, C., Smale, D., Thölix, L., and De Mazière, M.: Trends of ozone total columns and vertical distribution from FTIR observations at eight NDACC stations around the globe, Atmos. Chem. Phys., 15, 2915–2933, doi:10.5194/acp-15-2915-2015, http://www.atmos-chem-phys.net/15/2915/2015/, 2015.

Vyushin, D. I., Fioletov, V. E., and Shepherd, T. G.: Impact of long-range correlations on trend detection in total ozone, J. Geophys. Res., 10 112, n/a–n/a, doi:10.1029/2006JD008168, http://dx.doi.org/10.1029/2006JD008168, d14307, 2007.

Waters, J. W., Froidevaux, L., Harwood, R. S., Jarnot, R. F., Pickett, H. M., Read, W. G., Siegel, P. H., Cofield, R. E., Filipiak, M. J., Flower, D. A., Holden, J. R., Lau, G. K., Livesey, N. J., Manney, G. L., Pumphrey, H. C., Santee, M. L., Wu, D. L., Cuddy, D. T., Lay, R. R., Loo, M. S., Perun, V. S., Schwartz, M. J., Stek, P. C., Thurstans, R. P., Boyles, M. A., Chandra, K. M., Chavez, M. C., Chen, G.-S., Chudasama, B. V., Dodge, R., Fuller, R. A., Girard, M. A., Jiang, J. H., Jiang, Y., Knosp, B. W., LaBelle, R. C., Lam, J. C., Lee, K. A., Miller, D., 15 Oswald, J. E., Patel, N. C., Pukala, D. M., Quintero, O., Scaff, D. M., Snyder, W. V., Tope, M. C., Wagner, P. A., and Walch, M. J.: The Earth observing system microwave limb sounder (EOS MLS) on the Aura Satellite, IEEE Trans. Geosci. Rem. Sens., 44, 1075–1092, doi:10.1109/TGRS.2006.873771, 2006.

Wild, J. D. and Long, C. S.: A Coherent Ozone Profile Dataset from SBUV, SBUV/2: 1979 to 2016, in preparation, 2017.

WMO: Scientific Assessment of Ozone Depletion: 2006, Global Ozone Research and Monitoring Project-Report No. 50, WMO (World 20 Meteorological Organization), Geneva, Switzerland, https://www.esrl.noaa.gov/csd/assessments/ozone/, 2007.

WMO: Scientific Assessment of Ozone Depletion: 2010, Global Ozone Research and Monitoring Project-Report No. 52, WMO (World Meteorological Organization), Geneva, Switzerland, https://www.esrl.noaa.gov/csd/assessments/ozone/, 2011.

WMO: Scientific Assessment of Ozone Depletion: 2014, Global Ozone Research and Monitoring Project-Report No. 55, WMO (World Meteorological Organization), Geneva, Switzerland, https://www.esrl.noaa.gov/csd/assessments/ozone/, 2014.

25 Wolter, K. and Timlin, M. S.: El Niño/Southern Oscillation behaviour since 1871 as diagnosed in an extended multivariate ENSO index (MEI.ext), Int. J. Clim., 31, 1074–1087, doi:10.1002/joc.2336, http://dx.doi.org/10.1002/joc.2336, 2011.
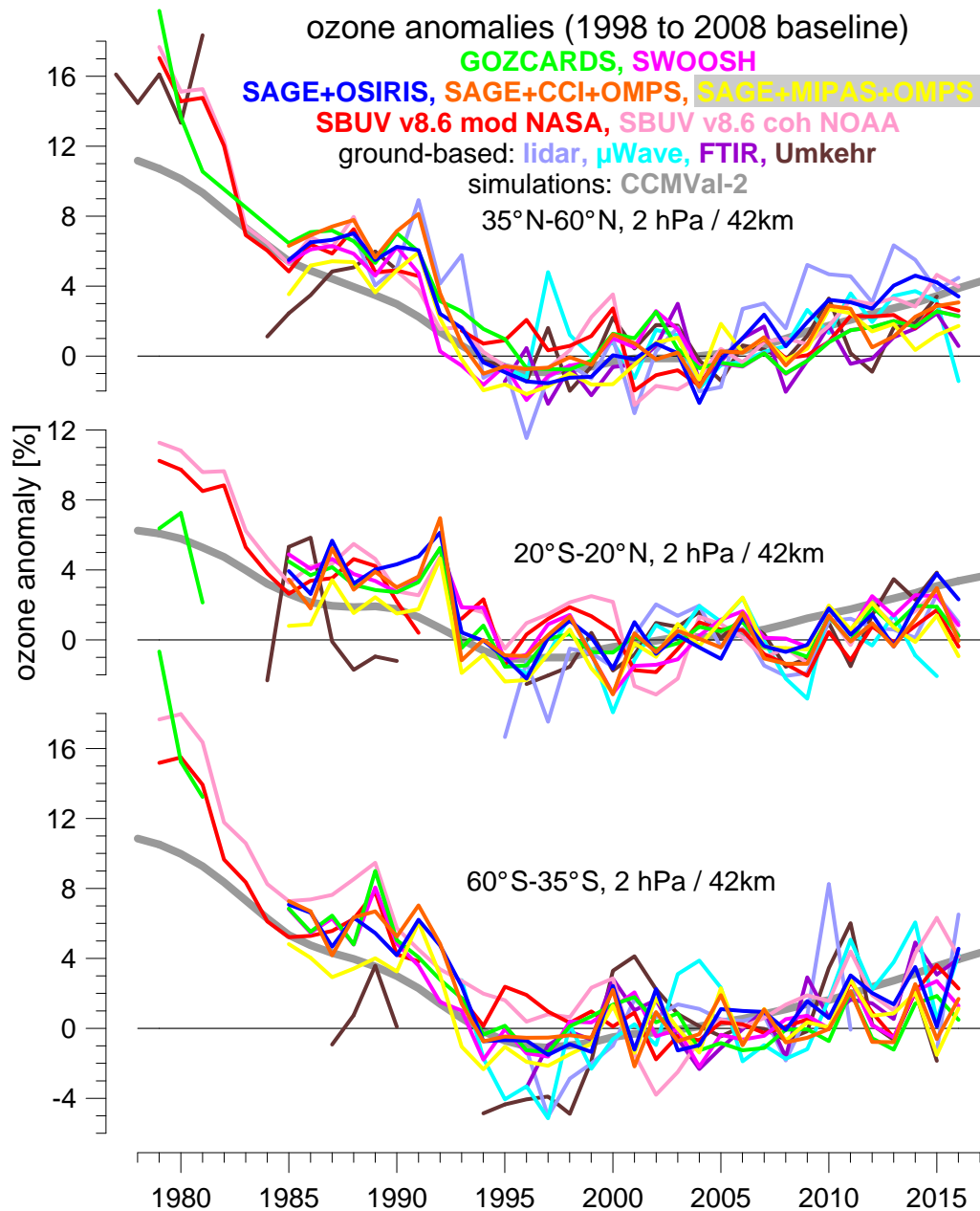
Figure 1. Annual mean ozone anomalies near 2 hPa or 42 km, as recorded by merged satellite data sets and NDACC ground-based stations. Anomalies are referenced to the 1998 to 2008 climatological annual cycle of each individual data set, and are averaged over the indicated zonal bands. NDACC stations close to a zonal band are also included, i.e. lidar data from Table Mountain at 34.4°N, FTIR data from Izaña at 28.3°N and Wollongong at 34.4°S, and Umkehr data from Perth at 34.7°S are included in the respective mid-latitude bands. The grey lines show corresponding ozone anomalies from CCMVal-2 model simulations (Eyring et al., 2010).
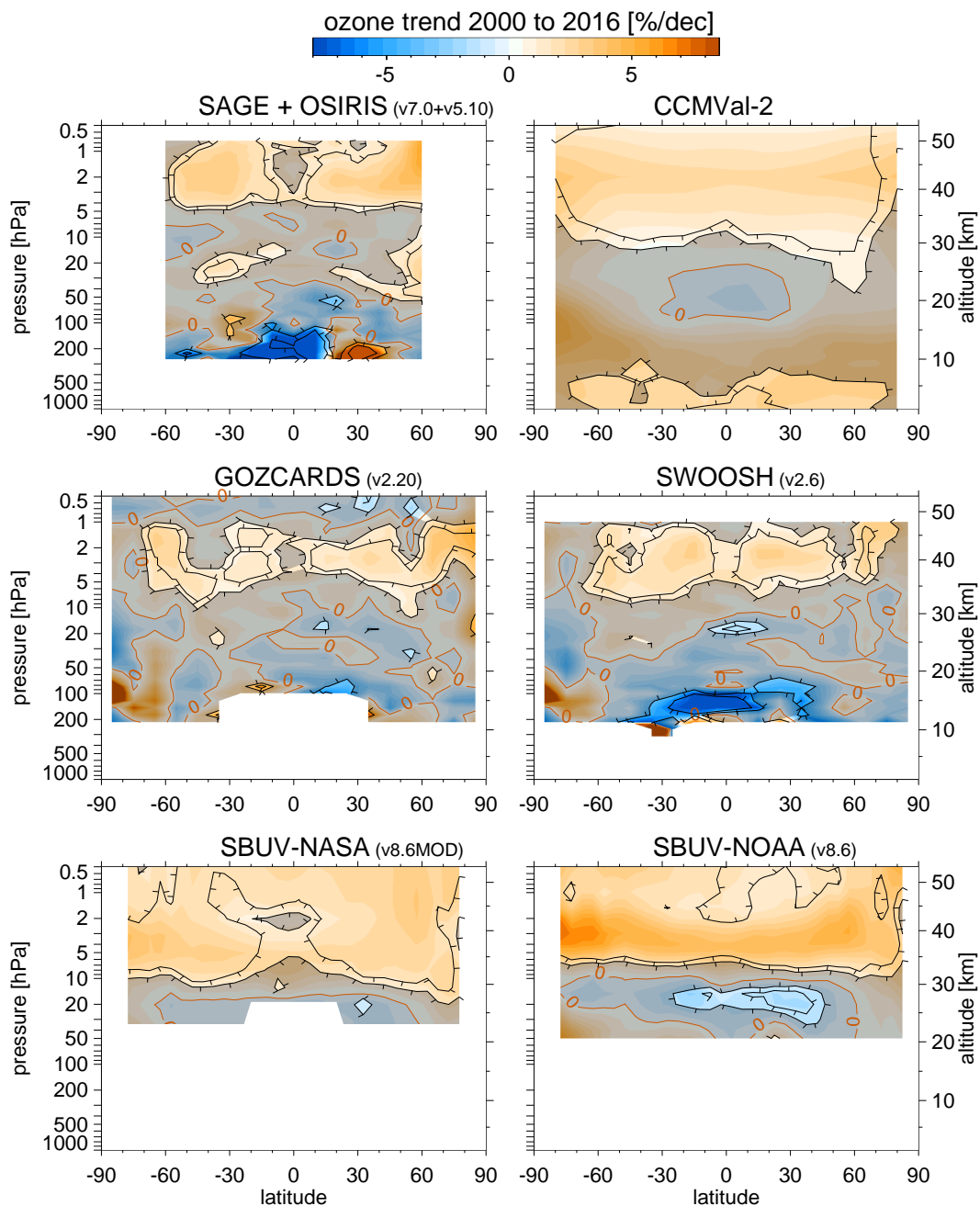
Figure 2. Latitude pressure cross section of 2000 to 2016 ozone trends TR obtained by 2-step multiple linear regression (see text). The top right panel is for model simulations from the CCMVal-2 initiative. The other panels are for merged satellite data sets. The colour scale gives trend magnitude TR. Shading and isolines give the ratio of trend to trend uncertainty, $|TR|/\sigma$. Grey shading, in regions where $|TR| \leq 2\sigma$, indicates that trends are not significant at the 95% confidence level. The next isoline is at $|TR|/\sigma = 3$.
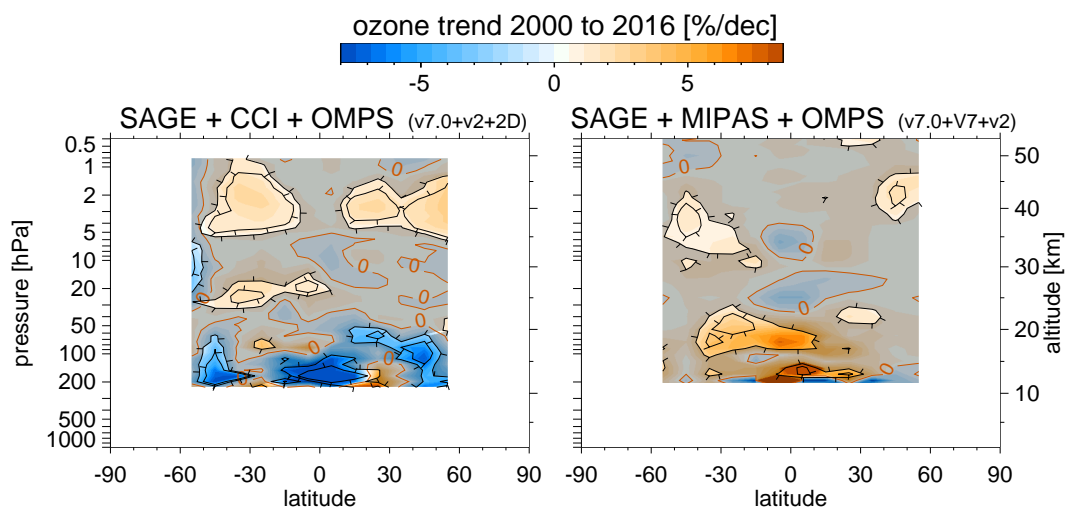
Figure 3. Same as Fig. 2, but showing the 2000 to 2016 ozone trends for the merged SAGE + ESA Ozone CCI + OMPS, and SAGE + MIPAS + OMPS data sets. The SAGE + ESA Ozone CCI + OMPS data set uses the OMPS 2D retrieval from U. Saskatoon. The SAGE + MIPAS + OMPS data set uses the OMPS v2 retrieval from NASA.
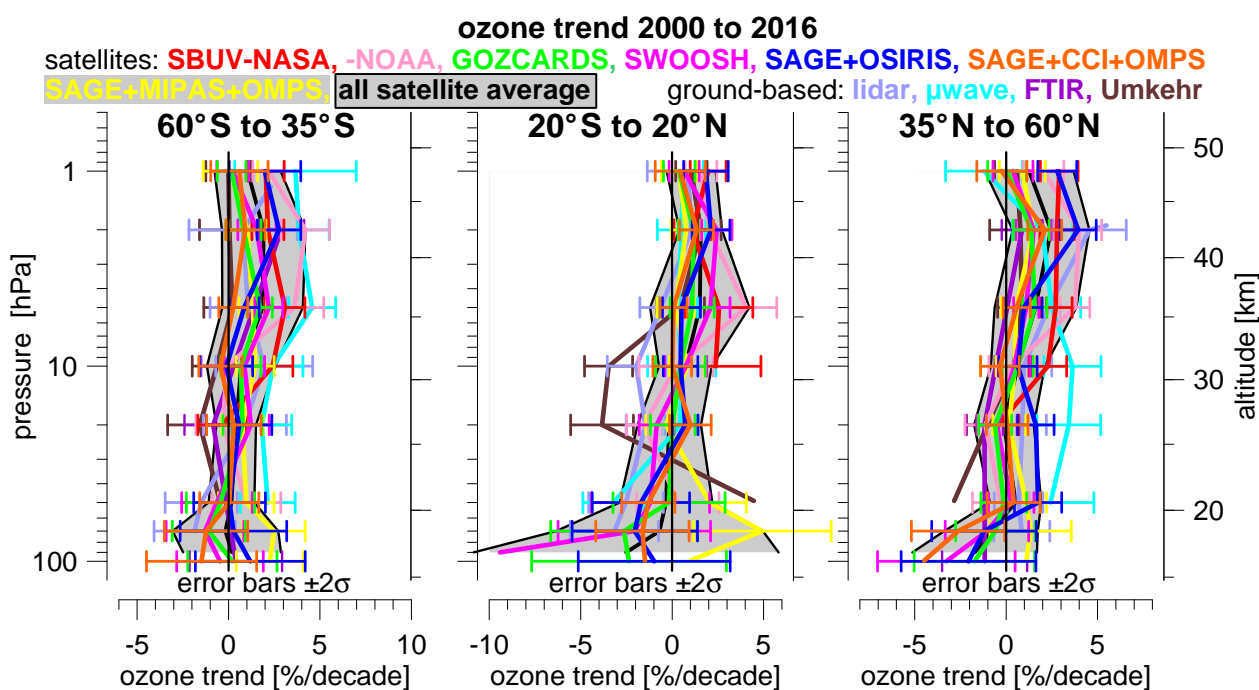
Figure 4. Vertical profiles of 2000 to 2016 ozone trends, obtained by 2-step multiple linear regression (see text), for different merged satellite and ground-based station data sets. Results are for the zonal bands 60°S to 35°S (left), 20°S to 20°N (center) and 35°N to 60°N (right). For the 60°S to 35°S zonal band, FTIR data from Wollongong (34.4°S), and Umkehr data from Perth (34.7°S) are included. For the 35°N to 60°N band, lidar data from Table Mountain (34.4°N) and FTIR data from Izaña (28.3°N) are included. SBUV and Umkehr data are not shown at/ below the 50 hPa level.
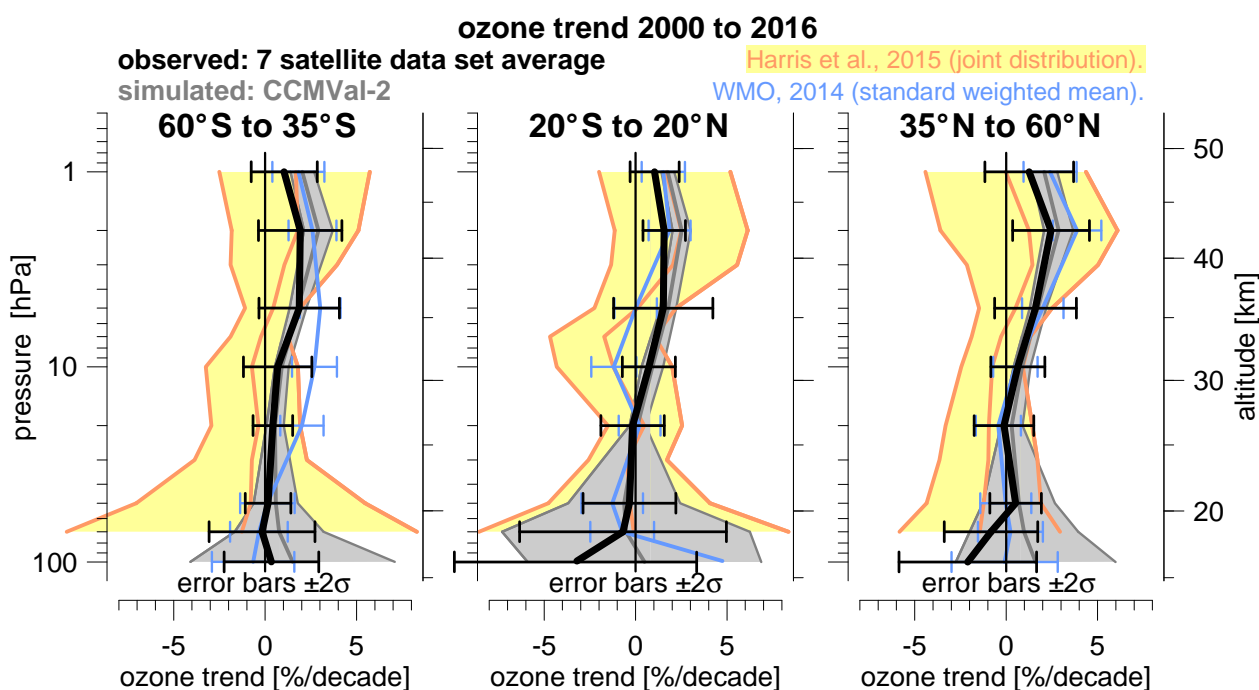
Figure 5. Same as Fig. 4, but giving the average 2000 to 2016 ozone trends (black lines) from seven merged satellite data sets (GOZCARDS, SWOOSH, SAGE + OSIRIS, SAGE + CCI + OMPS(2D), SAGE + MIPAS + OMPS(v2), SBUV-NASA, and SBUV-NOAA). SBUV trends are only used at levels above 40 hPa (23 km). Uncertainty bars and yellow shading give ±2 times the standard deviation σ of all individual trends in the average. For comparison, the 1998 to 2012 average ozone trend from Harris et al., 2015 (yellow lines and shading), and the 2000 to 2013 average ozone trend from WMO (2014) are shown as well. Grey lines and shading give corresponding trends and uncertainties from the CCMVal-2 model simulations.

Table 1. Merged satellite data sets used in the present study. The URLs serve as an entry point only, and do not always provide the newest and most complete data set used here. See text for references.

Name	Version(s)	from	to	URL
SBUV-NASA	v8.60MOD	05/1970 [a]	12/2016	https://acd-ext.gsfc.nasa.gov/Data_services/merged/
SBUV-NOAA	v8.60	11/1978	12/2016	ftp://ftp.cpc.ncep.noaa.gov/SBUV_CDR/
GOZCARDS	v2.20	02/1979 [b]	12/2016	https://gozcards.jpl.nasa.gov/
SWOOSH	v2.6	10/1984	12/2016	https://www.esrl.noaa.gov/csd/groups/csd8/swoosh/
SAGE II + OSIRIS (+ OMPS)[c,d]	v7.0 + v5.10 (+ 2D[d])	10/1984	12/2016	http://osirus.usask.ca/
SAGE II + Ozone_CCI + OMPS[d]	v7.0 + v2 + 2D[d]	10/1984	12/2016	http://www.esa-ozone-cci.org/
SAGE II + MIPAS + OMPS[e]	v7.0 + KIT v7 + v2[e]	10/1984 [f]	03/2017	https://www.imk-asf.kit.edu/english/304_2857.php

[a] gap from 05/1976 to 10/1978; [b] includes also SAGE I, but gap from 12/1981 to 09/1984, when SAGE II begins; [c] the SAGE + OSIRIS data set optionally includes OMPS data. These start in 04/2012, and give very similar trend results. However, to keep more independence between the various data sets, the version with OMPS data is not used here; [d] OMPS 2D retrieval from U. Saskatoon; [e] OMPS retrieval from NASA; [f] MIPAS high resolution data from 07/2002 to 03/2004, reduced resolution data from 01/2005 to 04/2012, gap in between.

Table 2. Stations and instruments used in the present study. Lidar, microwave and FTIR data are from the Network for the Detection of Atmospheric Composition Change (NDACC), and are originally available at http://www.ndacc.org. Umkehr data were provided by I. Petropavlovskikh.

Name	latitude	longitude	instrument	from	to
Fairbanks	64.8°N	147.9°W	Umkehr	03/1994	09/2015
Hohenpeissenberg	47.8°N	11.0°E	lidar	09/1987	12/2016
Bern	46.9°N	7.5°E	microwave	11/1994	12/2016
Payerne	46.8°N	7.0°E	microwave	01/2000	12/2016
Arosa	46.8°N	9.7°E	Umkehr	01/1956	12/2015
Jungfraujoch	46.6°N	8.0°E	FTIR	05/1995	11/2016
Haute Provence	43.9°N	5.7°E	lidar	07/1985	10/2016
Haute Provence	43.9°N	5.7°E	Umkehr	01/1984	11/2015
Boulder	40.0°N	105.3°W	Umkehr	01/1984	12/2015
Table Mountain	34.4°N	117.7°W	lidar	02/1988	09/2016
Izaña	28.3°N	16.5°W	FTIR	03/1999	10/2016
Mauna Loa	19.5°N	155.6°W	lidar	07/1993	09/2016
Mauna Loa	19.5°N	155.6°W	microwave	07/1995	05/2015
Mauna Loa	19.5°N	155.6°W	Umkehr	01/1984	12/2015
Wollongong	34.4°S	150.9°E	FTIR	05/1996	11/2016
Perth	34.7°S	138.6°E	Umkehr	01/1987	12/2015
Lauder	45.0°S	169.7°E	microwave	10/1992	10/2016
Lauder	45.0°S	169.7°E	lidar	11/1994	12/2016
Lauder	45.0°S	169.7°E	FTIR	10/2001	12/2016
Lauder	45.0°S	169.7°E	Umkehr	02/1987	12/2015

Table 3. Proxy time series used for the multiple linear regression in Eq. 2 in this study.

Proxy	description	URL
trend	linear increase over entire time period.	
change of trend	"hockey stick": 0 before 01/1997, linear increase after.	
QBO	10 and 30 hPa equatorial zonal wind from Singapore radio-sondes, as compiled by FU Berlin	http://www.geo.fu-berlin.de/en/met/ag/strat/produkte/qbo/index.html
Solar Cycle	solar radio flux at 10.7 cm, observed at Penticton, Canada.	ftp://ftp.geolab.nrcan.gc.ca/data/solar_flux
El-Nino	Multivariate ENSO index from Wolter and Timlin (2011).	https://www.esrl.noaa.gov/psd/enso/mei/
Aerosol	stratospheric aerosol optical depth following Sato et al. (1993).	https://data.giss.nasa.gov/modelforce/strataer/

Table 4. Average 2000 to 2016 ozone profile trends, obtained from individual trends for the GOZCARDS, SWOOSH, SAGE + OSIRIS, SAGE + CCI + OMPS(2D), SAGE + MIPAS + OMPS(v2), SBUV-NASA, and SBUV-NOAA satellite data sets. Given are mean trend TR and standard deviation 1σ of the individual trends, in percent per decade. Bold numbers indicate average trends TR larger than $2\sigma/\sqrt{3} \approx 1.15\sigma$, i.e. statistically significant with 95% confidence, assuming that the 7 data sets give 3 independent realizations of individual trends $TR(i)$. The SBUV-NASA and SBUV-NOAA data sets are used only at levels above 40 hPa (23 km). Therefore, $2\sigma/\sqrt{2} \approx 1.41\sigma$ is applied as threshold for bold face at the 50 and 70 hPa levels.

level	60°S to 35°S		20°S to 20°N		35°N to 60°N		60°S to 60°N	
(hPa)	TR	1σ	TR	1σ	TR	1σ	TR	1σ
1	**1.0**	0.9	**1.0**	0.7	**1.3**	1.2	**1.1**	0.7
2	**1.9**	1.1	**1.6**	0.6	**2.5**	1.1	**1.8**	0.6
5	**1.9**	1.1	1.5	1.4	**1.6**	1.1	**1.6**	1.2
10	0.7	0.9	0.7	0.7	0.6	0.7	0.8	0.7
20	0.4	0.5	-0.2	0.9	-0.1	0.8	0.0	0.7
50	0.2	0.6	-0.3	1.3	0.5	0.7	0.0	0.8
70	-0.2	1.4	-0.7	2.8	-0.8	1.3	-0.6	1.9

All values are % per decade.